Journal of Nuclear Materials 460 (2015) 16–22

Contents lists available at ScienceDirect

Journal of Nuclear Materials

journal homepage: www.elsevier.com/locate/jnucmat

Review

Radiation damage resistance and interface stability of copper–graphene nanolayered composite

Hai Huang [a], Xiaobin Tang [a,b,*], Feida Chen [a], Yahui Yang [a], Jian Liu [a], Huan Li [a], Da Chen [a,b]

[a] Department of Nuclear Science & Engineering, Nanjing University of Aeronautics and Astronautics, Nanjing 210016, China
[b] Jiangsu Key Laboratory of Nuclear Energy Equipment Materials Engineering, Nanjing 210016, China

ARTICLE INFO

Article history:
Received 22 November 2014
Accepted 2 February 2015
Available online 7 February 2015

ABSTRACT

The radiation damage resistance and interface stability of copper–graphene nanolayered composite are studied by atomistic simulations. Results show that the number of surviving point defects in bulk region is always less than that of pure copper at 100 K, when the range of initial distance d between a primary knock-on atom (PKA) with 3 keV and copper–graphene interface is less than 4 nm. The above phenomenon also occurs at 300, 500, and 700 K when d is ~15.4 Å, thereby implying that the composite resulting from copper–graphene interfaces exhibits excellent ability to resist radiation damage. A higher PKA energy corresponds to worse radiation damage of graphene in the composite. The damage may impair interface stability and eventually weaken the radiation damage resistance of the composite.

Contents

1. Introduction

The requirement of advanced nuclear energy systems for materials with significantly high radiation tolerance puts forward great challenges to currently available materials [1]. Vacancies and interstitials generated by displacement cascades under high-energy radiation in irradiation environments can aggregate to form defect clusters (interstitial clusters and voids, among others) within irradiated materials [2–5]. Ultimately, this condition results in swelling, hardening, and embrittlement that cause material failure [6]. Therefore, the effective removal of radiation-induced point defects is the key in improving the mechanical properties of irradiated materials.

Grain boundaries (GBs) and interfaces can act as sinks for all types of defects [1]. Studies of GBs and interfaces have recently focused on single-element nanostructured materials (SNM) and multilayer metallic composites (MMC), respectively [7]. Several SNMs have shown [8,9] that GBs are subjected to rapid grain growth during irradiation; this rapid grain growth can greatly weaken the radiation resistance of SNMs. In addition, research about MMC has demonstrated [10–13] that, unlike GBs in SNM,

* Corresponding author at: Department of Nuclear Science & Engineering, Nanjing University of Aeronautics and Astronautics, Nanjing 210016, China. Tel.: +86 13601582233; fax: +86 025 52112906 80407.
E-mail address: tangxiaobin@nuaa.edu.cn (X. Tang).

http://dx.doi.org/10.1016/j.jnucmat.2015.02.003
0022-3115/

interfaces in MMC are compositionally constrained against migration. However, only meeting these conditions, such as positive heat of mixing and non-tendency to form intermetallic compounds for two different kinds of metals in MMC, MMC can exhibit excellent radiation resistance [10,14]. In addition, the materials should not contain atoms that will become radioactive under neutron irradiation [14] because atoms dramatically affect the selection of MMC that act as nuclear engineering materials. Hence, novel approaches are necessary in designing materials to overcome the obstacles while maintaining the radiation resistance of MMC.

Graphene, which exhibits exceptional mechanical properties (Young's modulus of 1 TPa and ideal strength of 130 GPa), has been deemed as an excellent strength enhancer in composites [15]. The synthesis of metal–graphene nanolayered composites conducted by Kim et al. made possible enhancing metallic materials by interlayer graphene interfaces. Their study has shown that the strength and toughness of the composites are remarkably enhanced by the improved interface stability, which effectively removed interface dislocations through core dissociation processes [16]. As a result, all kinds of low activation metals may act as radiation tolerance materials by synthesizing metal–graphene nanolayered composites, which can get rid of the collocation restriction of constituent elements of MMC and augment the types of radiation tolerance materials.

In this work, molecular dynamics (MD) simulations were used to describe the effects of copper–graphene (Cu–C_gr) interfaces on reducing defects in a copper–graphene nanolayered composite (CGNC) system as it relates to radiation environments. In addition, the stability of Cu–C_gr interfaces related to the PKA energy was described. Two issues were addressed in this work: (1) CGNC, owing to the role of Cu–C_gr interfaces in acting as sinks for defects and which can resist radiation damage to some extent, and (2) the stability of Cu–C_gr interfaces, especially graphene, which is adversely affected by irradiation-induced collision cascades.

2. Simulation methods

The MD simulations were carried out using the public-domain molecular dynamics code LAMMPS [17]. The embedded-atom-method (EAM) interatomic potential, developed by Mishin et al., was used to describe the interactions between copper atoms (Cu–Cu) splined to the ZBL repulsive potential for interatomic distances less than 0.5 Å [18,19]. The interactions between carbon atoms (CzC) in graphene were described by the adaptive intermolecular reactive empirical bond order (AIREBO) potential as implemented in LAMMPS package with 2.0 Å as the cutoff distance [20,21]. In describing the interactions between copper and carbon atoms (Cu–C), 12–6 Lennard–Jones (LJ) type of van der Waal's interaction was used, where the well depth (ε) and equilibrium distance (σ) parameters derived from quantum level simulations [22] provide a reasonable approximation to the behavior of Cu–C interactions. The potential can be given by the equation

$$E = 4\varepsilon\left[\left(\frac{\sigma}{\bar{r}}\right)^{12} - \left(\frac{\sigma}{\bar{r}}\right)^{6}\right], \quad (\bar{r} < r_c)$$

and the LJ parameters with $\varepsilon_{(Cu-C)} = 0.0117$ eV, $\sigma_{(Cu-C)} = 3.0023$ Å, and the cutoff $r_c = 2.5\sigma_{(Cu-C)}$.

There are three configurations with different stacking orders for the interfacial structure of Cu–C_gr, namely, graphene-C-A (topfcc), graphene-A-B (tophcp) and graphene-B-C (hcpfcc) [23], as shown in Fig. 1(a). In this work, the graphene-C-A (topfcc) configuration which has the lowest energy and is thus the most stable one was chosen as shown in Fig. 1(b) and (c), and has been extensively investigated in the past [22,23].

The simulations investigated the effect of interfaces of CGNC on defects reduction by two factors. These factors are the initial distance d between a PKA and Cu–C_gr interface and the temperature T of the environment. A CGNC system measuring 155.10 × 119.35 × 166.54 Å^3 (264,044 atoms) served as simulation cell for this study, in which each layer thickness of copper is approximately 80 Å, and both of the crystallographic orientations of copper are x [−110], y [−1−12], z [111], as shown in Fig. 2(a). The graphene sheet measured 155.10 Å (zigzag direction) × 119.35 Å (armchair direction). In addition, given the relatively small number of atoms used in the simulations, the system was simulated using periodic boundary conditions (PBC) along the three directions. The simulations were carried out as follows. (**1**) At the beginning, the system was relaxed at the NVT ensemble (T = 100 K) with a time step (Δt) of 10^{-3} ps for 10 ps until the system reached a stable state. Then, a PKA of 3.0 keV was introduced at varying distances away from and directed toward the interface, which induced a collision cascade with the Δt of 10^{-5} ps for 1 ps and an additional 5 ps with a larger Δt of 10^{-4} ps. At this stage, atoms within the "thermostat region" were forced to maintain a constant temperature of 100 K through the Nose–Hoover heat bath, such that the excess kinetic energy introduced by the PKA could be dissipated as in experimental situations. Atoms within the "active region" were restricted to move adiabatically (the NVE ensemble), as shown in Fig. 2(b). Eventually, the Δt was increased back to 10^{-3} ps for 60 ps to further anneal the system. As an example, snapshots of the above simulation process where a PKA was placed at d = 15.4 Å are shown in Fig. 3, in which the cascade reaches its maximum extent near the interface after 0.5 ps, and the cascade annealing is close to completion after 4 ps. (**2**) The CGNC was also investigated at other three temperatures, namely 300, 500, and 700 K. The details of simulations at the three

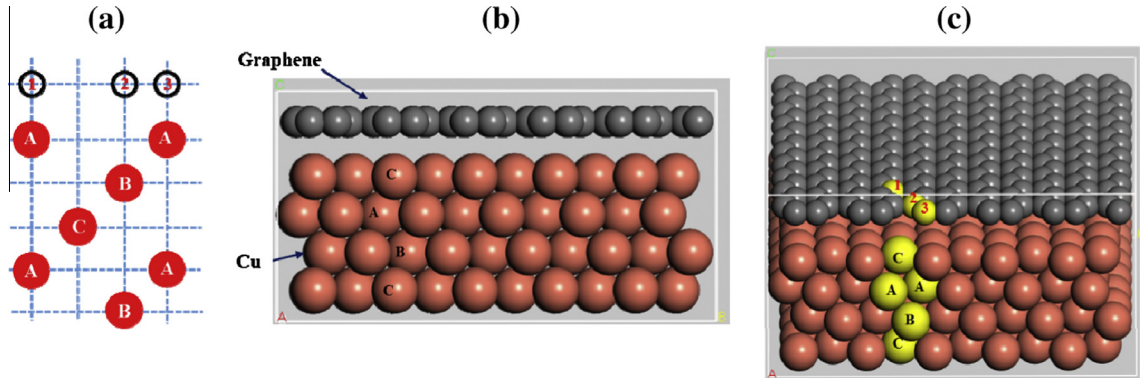

Fig. 1. (a) Schematic representation of atomic structure of the interface and Cu substrate represented by four atomic layers. A, B and C represent copper atoms in different atom layers. 1, 2 and 3 represent carbon atoms in different position of graphene; (b) The front view of graphene-C-A (topfcc); (c) The top view of graphene-C-A (topfcc).

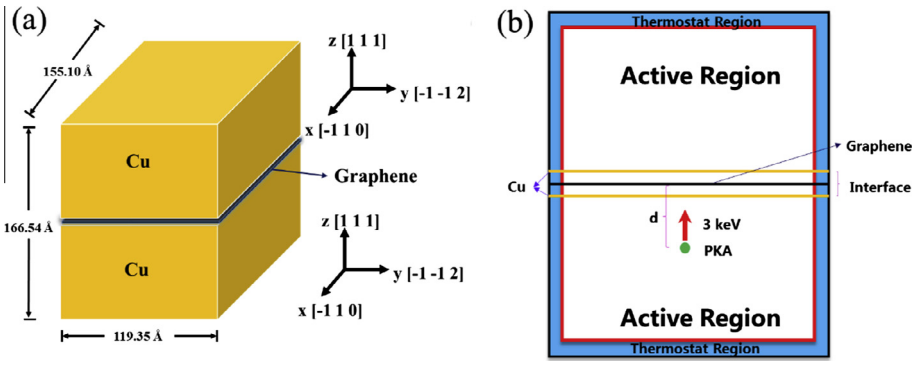

Fig. 2. (a) Crystallographic orientation and size of CGNC used as simulation cell for the first study; (b) The MD configuration viewed in the *x*-direction. Atoms within the "thermostat region" (along the three directions) are controlled by NVT thermostat to maintain a constant temperature. Other atoms (within the "active region") are allowed to move adiabatically as NVE ensemble. In the simulation cell, the three directions exhibit PBC, and the PKA with energy of 3 keV is at a distance away from the Cu–C_gr interface.

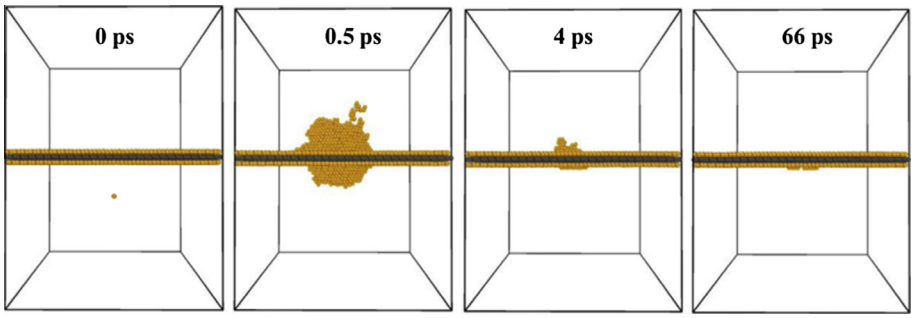

Fig. 3. Snapshots of MD simulation process. The PKA is placed 15.4 Å from the interface along the *z*-axis. Yellow spheres represent copper atoms, and gray spheres represent carbon atoms. After relaxation and heating, a collision cascade is created at 0 ps, and the cascade reaches its maximum size after 0.5 ps. (For interpretation of the references to color in this figure legend, the reader is referred to the web version of this article.)

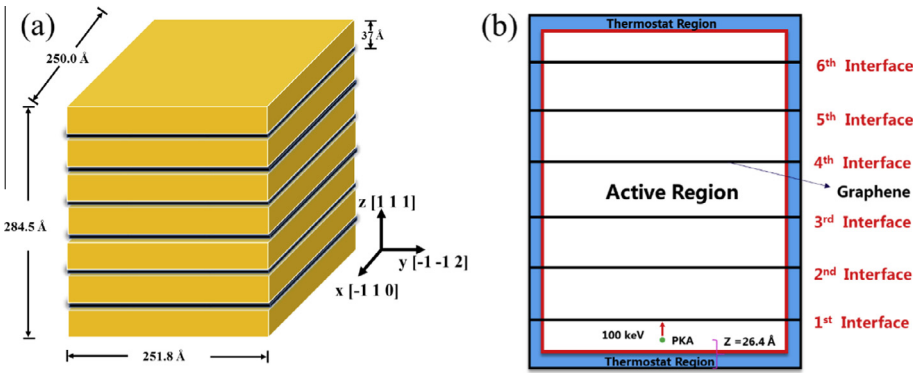

Fig. 4. (a) Crystallographic orientation and size of CGNC used as simulation cell for the second study; (b) The MD configuration viewed in the *x*-direction. (The same description as Fig. 1(b).)

temperature, such as simulation time, the energy and direction of PKA, ensemble and so on, were similar to those of the simulations at varying distance *d* as shown above; the distance of PKA-interface at the three temperature was definitely picked $d = 15.4$ Å.

In illustrating the stability of Cu–C_gr interfaces related to the energy of a PKA, a larger CGNC system measuring $250 \times 251.8 \times 284.5$ Å^3 (1,553,520 atoms) and containing six interfaces served as simulation cell for this study. Each copper layer has a thickness of 37 Å, as shown in Fig. 4(a). A PKA of 100 keV was introduced at $Z = 26.4$ Å and directed toward the interface; the details of simulation were similar to those of the simulations at varying distance *d* as shown above, but the system "annealing" was 200 ps, as shown in Fig. 4(b).

3. Results and discussion

3.1. Interfacial width of CGNC

Interfacial width should be defined in studying the effects of Cu–C_gr interfaces on the point defects in the bulk region. In this work, the potential energy of the atoms close to copper–graphene interfaces were used to define interfacial width [24], based on the atomistic model. The potential energy of atoms close to Cu–C_gr interfaces differed clearly from that of atoms in the bulk. The cohesive energy of a copper atom in pure copper derived from the potential is equal to −3.54 eV; the calculations predict that a CGNC atom whose potential energy is equal to the value should be in the

bulk. Interfacial width is defined in this study as the region near the diving interface, which includes atoms with a potential energy not in the interval -3.54 ± 0.01 eV.

Fig. 5 shows the average potential energy of atoms belonging to the simulation cell as a function of the perpendicular distance from the interface, which is symmetrical at 83.7 Å. Based on the used definition, interfacial width is approximately 6 Å; this width contains the graphene and two terminal copper planes near the graphene. Conversely, the region which is 3 Å or farther from the center of the interface (at $Z = 83.7$ Å) is considered as the bulk region.

The reference lattice site method [18] with a cutoff distance of $0.3a_0$ (a_0 is the lattice constant of copper) was used to characterize point defects and count the number of point defects surviving in the bulk region. If defects form a cluster, only the net number of defects were counted. For example, three vacancies and one SIA in a cluster after the cascade cools down were treated as two vacancies.

3.2. Radiation damage resistance of CGNC

3.2.1. Point defects in the bulk region due to distance d

If the number of surviving point defects in the bulk region where a PKA was introduced at varying distances away from the Cu–C_gr interface is less than that of pure copper with simulations similar to CGNC, then CGNC should be able to resist damage resistance, and vice versa. Thus, the initial distance of PKA from the Cu–C_gr interface, which may cause a difference in point defects, is a characterization for the radiation damage resistance of CGNC, and very necessary to study.

Fig. 6 shows the number of surviving point defects (interstitials and vacancies) in the bulk region as a function of d. Each data point in Fig. 6 (and thereafter) is an averaged value of 10 independent MD runs in the system to improve statistics. The number of interstitials in pure copper where the orientation and energy of a PKA are consistent with those of the CGNC simulations is 7.8 ± 1.23; this value is shown for comparison. In Fig. 6, the number of surviving point defects in the bulk region, either interstitials or vacancies, is substantially less than the average of 7.8 interstitials surviving in pure copper. Clearly, the defects are sensitive to d and tend to increase with d. In other words, the difference of the number of defects between the bulk region and pure copper, especially vacancies, gradually decreases when d increases. As d becomes sufficiently large, the number of defects is presumed to approach the value of pure copper, thereby suggesting that Cu–C_gr interfaces that act as sinks play an important role in facilitating the recombination and annihilation of the point defects of the bulk region created during irradiation-induced collision cascades, and that CGNC, to some extent, is able to resist radiation damage unlike pure copper. In addition, the number of vacancies over the entire range of d (except 5 Å) is more than that of interstitials, as shown in Fig. 6, thus implying that the interface preferentially absorbs interstitials over vacancies.

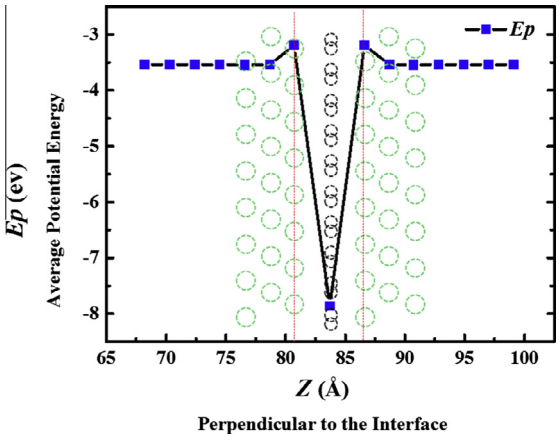

Fig. 5. Average potential energy of atoms near the interface parallel to the interface as a function of the coordinate perpendicular to the interface. Green circles represent copper atoms and gray circles represent carbon atoms; the range between the two red lines represents interfacial width. (For interpretation of the references to color in this figure legend, the reader is referred to the web version of this article.)

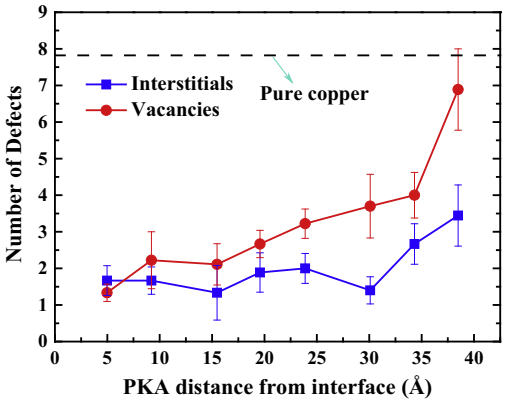

Fig. 6. Number of surviving point defects induced by a 3 keV PKA in the bulk region at 100 K, as a function of PKA distance from the interface. The number of interstitials (or vacancies) in pure copper where the orientation and energy of a PKA are consistent with those of the CGNC simulations is indicated by the horizontal dashed line. (Note that in pure copper, the number of vacancies and interstitials are equal.)

3.2.2. Point defects in the bulk region due to temperature T

Temperature, a key factor that affects the evolution of radiation-induced defects in materials, is related to the radiation damage resistance of materials. Thus, investigating the effects of temperature on reducing defects in CGNC is particularly important. A certain d at 15.4 Å was randomly selected; it is the initial distance between a 3 keV PKA and the interface, and was used to investigate the effects of T on the ability of CGNC to reduce radiation damage. The number of interstitials in pure copper where the orientation and energy of a PKA are consistent with those of the CGNC simulations in different temperatures is also shown for comparison.

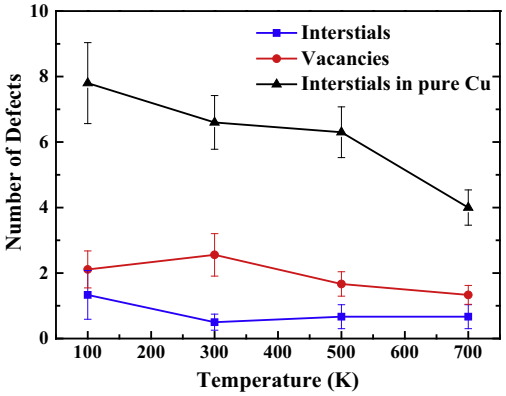

Fig. 7. Number of surviving defects in the bulk region, generated by a 3 keV PKA away from the interface about 15.4 Å, as a function of temperature. The number of interstitials (or vacancies) in pure copper where the orientation and energy of a PKA are consistent with those of the CGNC simulations is indicated by the solid black line.

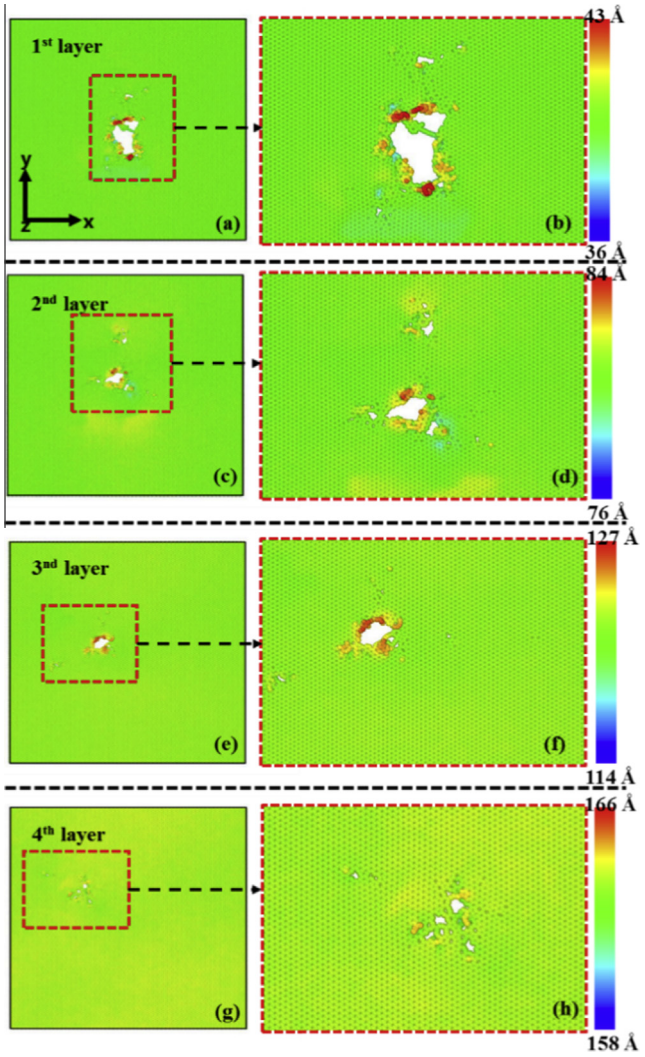

Fig. 8. Effects of the displacement cascades generated by a 100 keV PKA on the different layers of graphene of CGNC, viewed in the *z*-direction. Figures (b), (d), (f), and (h) are the locally enlarged figure as the red-dotted rectangles shown in (a), (c), (e), and (g), respectively. Carbon atoms in each graphene are colored according to their *z*-coordination. (For interpretation of the references to color in this figure legend, the reader is referred to the web version of this article.)

As illustrated in Fig. 7, the number of point defects in the bulk region, either interstitials or vacancies, is less than that of pure copper in each *T*, thereby suggesting that the interface facilitates the recombination or absorption of the point defects of the bulk region. The number of point defects in pure copper is related to *T* and tends to decrease when *T* increases; this finding agrees with the findings of Gao et al. in their study of α-iron [25]. However, the number of point defects in the bulk region is almost not affected by *T*; the fluctuation is less than 1, thus implying a connection between Cu–C_gr interfaces and temperature to balance the number of point defects in the bulk region. In addition, the number of vacancies is more than that of interstitials in the bulk region.

3.3. Interface stability of CGNC due to irradiation

The displacement cascades generated by a PKA greatly affects the stability of Cu–C_gr interfaces, which may weaken the radiation damage resistance of CGNC, hence the importance of investigating the stability of Cu–C_gr interfaces affected by collision cascades. In addition, the graphene of CGNC may be induced to crack during irradiation and thus lead to the breakdown of the layered morphology of CGNC by displacing atoms ballistically or by creating transient pockets of molten material where rapid interdiffusion takes place [26]. Eventually, the copper atoms at the top and the bottom of graphene may recrystallize to form a columnar block through the break of graphene, reduce the interfacial area, and impair the stability of Cu–C_gr interfaces. Therefore, the stability of Cu–C_gr interfaces should mainly focus on the radiation damage resistance of graphene in CGNC.

The effects of the displacement cascades generated by a high-energy PKA on the graphene of CGNC were used in the qualitative analysis of radiation damage resistance of graphene. At 100 K, the simulation of displacement cascades being generated by a 100 keV PKA was carried out in the six–interface system, as depicted in Fig. 4(b). As the simulation time went on, the energy of PKA directed toward the interfaces gradually decreased. In Fig. 8, the damage of graphene diminishes as the PKA energy gradually decreases and by the end of the fourth layer graphene. In addition, the large breaks in the first four layer of graphene are very difficult to restore, and the higher PKA energy exhibits larger breaks. Such breaks cause the copper atoms at the top and the bottom of graphene to recrystallize and form a columnar block through breaks, as shown in Fig. 9; as the PKA energy decreased gradually, the recrystallization of the copper atoms at the top and the bottom of graphene also diminished.

The damage of graphene generated by a 3 keV PKA at 100 K, which is away from Cu–C_gr interface at 15.4 Å in the single-interface system (Fig. 2), was also studied. At 0 ps, the graphene remains intact, as shown in Fig. 10(a) and (b). After 0.5 ps, the number of the carbon atoms in the graphene displaced from their

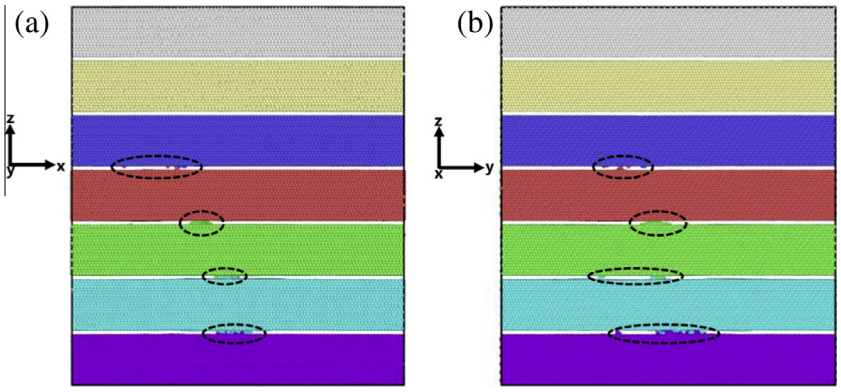

Fig. 9. Effects of the displacement cascades generated by a 100 keV PKA on the different layers of copper near the Cu–C_gr interfaces in CGNC, viewed in the *y*-direction (a) and *x*-direction (b), which hide the graphene layers. The different colors of copper atoms represent copper atoms in different Cu layers along *z*-direction. The regions in the black ovals represent the recrystallization of the copper atoms at the top and the bottom of graphene. (For interpretation of the references to color in this figure legend, the reader is referred to the web version of this article.)

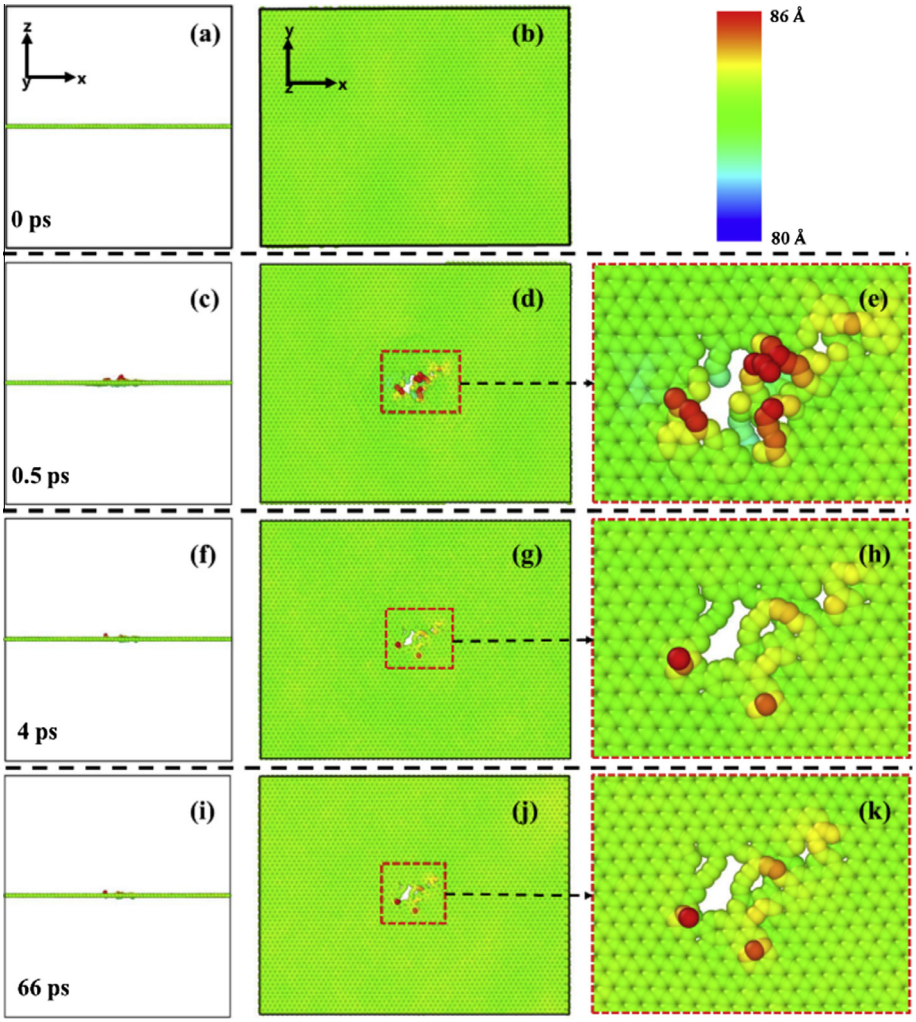

Fig. 10. Snapshots of MD simulation process of the graphene in the single-interface system generated by a 3 keV PKA, viewed in the *y*-direction (figures (a), (c), (f), and (i)) and *z*-direction (figures (b), (d), (g), and (j)). Figures (e), (h), and (k) are the locally enlarged figure as the red-dotted rectangles shown in (d), (g), and (j), respectively. Carbon atoms in the graphene are colored according to their *z*-coordination. (For interpretation of the references to color in this figure legend, the reader is referred to the web version of this article.)

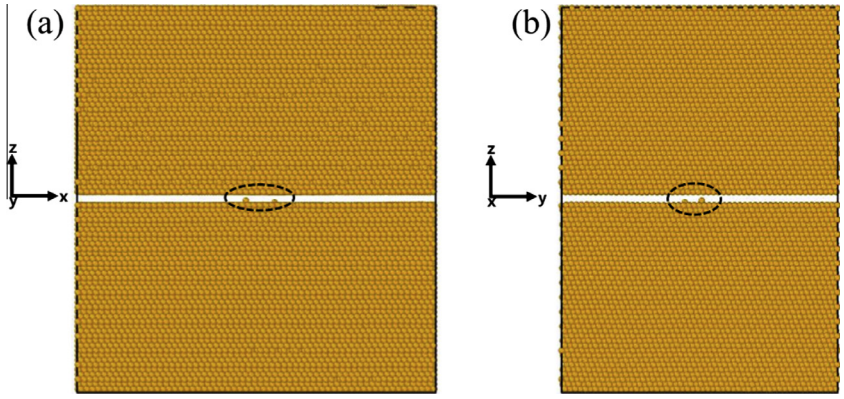

Fig. 11. Effects of the displacement cascades generated by a 3 keV PKA on the copper atoms near Cu–C_gr interface in single interface system, viewed in the *y*-direction (a) and *x*-direction (b), which hide the graphene. The regions in the black ovals black ovals represent the recrystallization of the copper atoms at the top and the bottom of graphene.

normal lattice sites reaches its maximum, thus leaving a small break in the graphene, as shown in Fig. 10(c)–(e). With the annealing, part of the dislocated carbon atoms would return to the normal site of the graphene; self-healing occurs and reaches stability after 4 ps, as shown in Fig. 10(f)–(k). Further simulations show that the self-healing of graphene similar to the above occurs in the six-interface system, but the breaks are too large to restore (Fig. 8(a)–(h)). In addition, the tendency to form a columnar block in the interface area does not occur in spite of the break, as depicted in Fig. 11, thereby suggesting that the effects of the

displacement cascades caused by a low-energy PKA on the graphene are limited.

4. Conclusions

Molecular dynamics simulations were performed to investigate the radiation damage resistance and interface stability of CGNC. In order to count the number of surviving point defects in the bulk region, the width of Cu–C_gr interface was calculated (approximately 6 Å) and the result suggests that Cu–C_gr interface contains the graphene and two terminal copper planes near the graphene. The number of surviving point defects in the bulk region is always less than that of pure copper at 100 K, when the range of initial distance d between a PKA with 3 keV and Cu–C_gr interface is less than 4 nm. The orientation and energy of PKA in pure copper simulations are consistent with those of the CGNC simulations. Furthermore, the above phenomenon also occurs at 300, 500, and 700 K when d is 15.4 Å. These findings imply that Cu–C_gr interfaces can act as sinks and play an important role in facilitating the recombination and annihilation of the point defects of the bulk region created during collision cascades; thus, CGNC exhibits, to some extent, the ability to resist radiation damage. In addition, the displacement cascades generated by a PKA would have an effect on the graphene of CGNC; the higher the PKA energy, the worse the graphene of CGNCs subjected to radiation damage. The damage may lead the copper atoms at the top and the bottom of graphene to recrystallize and form a columnar block through the break of the graphene, thus impairing interface stability and eventually weakening the radiation damage resistance of the composites.

Acknowledgements

This work was supported by the Specialized Research Fund for the Doctoral Program of Higher Education of China (Grant No. 20133218110023), China Postdoctoral Science Foundation (Grant No. 2014M561642), the Jiangsu Planned Projects for Postdoctoral Research Funds (Grant No. 1401091C), the Foundation of Graduate Innovation Center in NUAA (Grant No. kfjj201443), the Fundamental Research Funds for the Central Universities and the Priority Academic Program Development of Jiangsu Higher Education Institutions.

References

[1] G. Ackland, Science 327 (2010) 1587–1588.
[2] B.D. Wirth, Science 318 (2007) 923–924.
[3] K. Arakawa, K. Ono, M. Isshiki, K. Mimura, M. Uchikoshi, H. Mori, Science 318 (2007) 956–959.
[4] Y.-H. Yang, X.-B. Tang, F.-D. Chen, H. Huang, J. Liu, Sci. China Technol. Sci. 57 (2014) 29–34.
[5] D.-K. Song, X.-G. Li, J.-M. Xue, H.-L. Duan, Z.-H. Jin, Philos. Mag. Lett. 94 (2014) 361–369.
[6] T.D. de la Rubia, H.M. Zbib, T.A. Khraishi, B.D. Wirth, M. Victoria, M.J. Caturla, Nature 406 (2000) 871–874.
[7] M.G. McPhie, L. Capolungo, A.Y. Dunn, M. Cherkaoui, J. Nucl. Mater. 437 (2013) 222–228.
[8] D. Kaoumi, A.T. Motta, R.C. Birtcher, J. Appl. Phys. 104 (2008) 073525.
[9] E. Beamish, C. Campañá, T.K. Woo, J. Phys.: Condens. Matter 22 (2010) 345006.
[10] A. Misra, M.J. Demkowicz, X. Zhang, R.G. Hoagland, JOM 59 (2007) 62–65.
[11] X.-Y. Liu, B.P. Uberuaga, M.J. Demkowicz, A. Misra, M. Nastasi, Phys. Rev. B 85 (2012) 012103.
[12] F.-D. Chen, X.-B. Tang, Y.-H. Yang, H. Huang, D. Chen, J. Nucl. Mater. 452 (2014) 31–36.
[13] Q.-M. Wei, Y.-Q. Wang, M. Nastasi, A. Misra, Phil. Mag. 91 (2011) 553–573.
[14] H.-X. Zhang, M.-Q. Hong, X.-H. Xiao, F. Ren, C.-Z. Nucl. Phys. Rev. 30 (2013) 451–459.
[15] X.-Y. Liu, F.-C. Wang, H.-A. Wu, W.-Q. Wang, Appl. Phys. Lett. 104 (2014) 231901.
[16] Y. Kim, J. Lee, M.S. Yeom, J.W. Shin, H. Kim, Y. Cui, J.W. Kysar, J. Hone, Y. Jung, S. Jeon, S.M. Han, Nat. Commun. 4 (2013) 2114.
[17] S. Plimpton, J. Comput. Phys. 117 (1995) 1–19.
[18] X.-M. Bai, A.F. Voter, R.G. Hoagland, M. Nastasi, B.P. Uberuaga, Science 327 (2010) 1631–1634.
[19] M.J. Demkowicz, R.G. Hoagland, Int. J. Appl. Mech. 1 (2009) 421–442.
[20] X. Wu, H.-Y. Zhao, M.-L. Zhong, H. Murakawa, M. Tsukamoto, Carbon 66 (2014) 31–38.
[21] L. Liang, S.-J. Zhao, Y.-G. Wang, J.-M. Xue, Acta Scientiarum. Naturalium. Un. 49 (2013) 365–370.
[22] L. Adamska, Y. Lin, A.J. Ross, M. Batzill, I.I. Oleynik, Phys. Rev. B 85 (2012) 195443.
[23] R. Mao, B.-D. Kong, C. Gong, S. Xu, T. Jayasekera, K. Cho, K.W. Kim, Phys. Rev. B 87 (2013) 165410.
[24] F.J. Pérez-Pérez, R. Smith, Nucl. Instrum. Meth. B 164 (2000) 487–494.
[25] F. Gao, D.J. Bacon, P.E.J. Flewitt, T.A. Lewis, J. Nucl. Mater. 249 (1997) 77–86.
[26] L. Zhang, M.J. Demkowicz, Appl. Phys. Lett. 103 (2013) 061604.